

Electronic spectroscopy of benzo[*g,h,i*]perylene and coronene inside helium nanodroplets

Özgür Birer,^{ab} Paolo Moreschini^b and Kevin K. Lehmann^{*c}

Received 8th November 2007, Accepted 4th January 2008

First published as an Advance Article on the web 5th February 2008

DOI: 10.1039/b717307e

We have recorded the electronic spectra of benzo[*g,h,i*]perylene and coronene and their van der Waals complexes with argon and oxygen with a helium-nanodroplet depletion spectrometer. These molecules differ by the addition of one and two fused benzene rings to perylene, which was previously studied in helium. The coronene spectrum is similar to a previously reported jet-cooled laser-induced fluorescence (LIF) spectrum. The van der Waals complexes with argon and oxygen show different complexation sites and maximum number of adsorbants. We report a vibronically resolved benzo[*g,h,i*]perylene $S_1 \leftarrow S_0$ spectrum. The spectral lines are split in a similar way to that of several molecules studied before. However, surprisingly, while the van der Waals complexes with argon are free of the splitting, the complexes with oxygen retain the splitting, with increased linewidth and splitting. We could also observe the $S_2 \leftarrow S_0$ origin transition of benzo[*g,h,i*]perylene which was previously observed by cavity ring down spectroscopy. While in general the two spectra are quite similar, the relative intensities and spectral shifts of several lines are different.

1. Introduction

The electronic spectroscopy of polycyclic aromatic molecules

(*i.e.* benzene,^{1,2} naphthalene,³ anthracene,⁴ tetracene,^{5–10} pen-

tacene,^{5,9,10} PTCDA,¹¹ porphyrin,^{9,12} phthalocyanines,^{13–16} cyanines,^{7,246 01} J. 344 Tj 5752 0 8 391. 5779 T4

Chillier. Tan and Salama confirmed that the $S_1 \leftarrow S_0$ transition carried a much smaller (2.7×10^{-4}) intrinsic oscillator strength compared to that of the $S_2 \leftarrow S_0$ transition (0.27) with their calculations. They have also reported that the S_1 state should have 1A_1 symmetry and the S_2 state should have 1B_1 symmetry. However, they have calculated the vertical transition energies of the S_1 and S_2 states as 27 217 and 27 401 cm^{-1} respectively, scanned this spectral window and concluded that the S_1 state was too weak to be observed. At the time when we observed the $S_1 \leftarrow S_0$ and $S_2 \leftarrow S_0$ transitions of BghiP in helium nanodroplets with depletion detection,³⁰ the high-resolution gas-phase $S_1 \leftarrow S_0$ spectrum did not exist in the literature. Recently, the cavity ring down and matrix-isolation $S_1 \leftarrow S_0$ spectra of BghiP were published.³¹ In this article, we present our findings and compare them to the gas-phase measurements. Our signal-to-noise ratio is superior to these gas-phase measurements where the assignments are mostly based on a difference spectrum.

Coronene belongs to the *peri*-condensed series of polyaromatic hydrocarbons. The symmetry of both the ground and first excited state is D_{6h} and this is responsible for many similarities between the spectra of coronene and benzene. Its first three excited singlet states (${}^1B_{2u}$, ${}^1B_{1u}$, ${}^1E_{1u}$), which are due to the $\pi \rightarrow \pi^*$ transitions between the HOMO (e_{2u}) and LUMO (e_{1g}), are generated after taking electron repulsion through configuration interaction into account. The $S_1 \leftarrow S_0$ transition is electronically forbidden; it becomes vibronically allowed with e_{2g} and b_{1g} modes polarized parallel and perpendicular to the plane of the molecule respectively. The latter transitions are, however, much weaker for polyaromatic hydrocarbons and are not observed. Because of the larger size of coronene the S_1 has lower energy than in benzene, with the first electronic transition showing in the blue end of the visible spectrum whereas the same system lies at 260 nm in the case of benzene. Also, the larger size of coronene is responsible for a larger number of normal modes (102 vs. 30) which complicates the spectrum.

The spectrum of coronene isolated in Shpol'skii matrices has been published by several groups.^{24,26,32} The jet-cooled coronene³³ and coronene- d_{12} ³⁴ spectra have been reported by Bermudez and Chan using the LIF method.

2. Experimental

The experiments were carried out on the Princeton droplet spectrometer, which was described in detail previously.^{19,35} The spectrometer has two differentially pumped chambers, each evacuated by oil diffusion pumps. A 10-micrometer nozzle in the source chamber is cooled down to 17 K by closed-cycle refrigerators. Helium gas at 50 bar pressure is expanded into vacuum to form droplets with a calculated mean size of 6500 atoms per droplet.³⁶ A 390- μm diameter skimmer is located about 1 cm from the nozzle, leading into the detection chamber. In that chamber, there are 2 ovens and 1 gas scattering box (each 2.5 cm long) used as pickup cells to load the droplets with the dopant(s) under study. The organic molecules (>98%, Aldrich) are heated (150–200 °C) in the ovens to a vapor pressure of about 10^{-4} Torr. The gas pickup cell is used to create the van der Waals complexes of the

organics with argon or oxygen. The pressure of the gas line is measured outside the chamber before a variable leak valve. Therefore, the recorded pressure is only proportional to the actual pressure inside the pickup cell and the absolute values should only be compared within individual experiments. The doped droplets interact with the laser in a multipass cell, which is composed of two flat high-reflector mirrors. The detector is an optothermal bolometer³⁷ which monitors the flux of the droplet beam. The droplet beam signal is ~ 13 mV, detected with a chopping frequency of 21 Hz. When an electronically excited molecule relaxes radiatively (nonradiatively) from the excited state, it imparts a fraction (all) of its excitation energy to the droplet causing evaporation and shrinkage in size. (In the radiative case, the droplet's deposited energy arises from the Stokes shift on emission.) The heat of evaporation of helium is ~ 5 cm^{-1} per atom and thus the droplets will essentially be completely evaporated away by an energy input of $\sim 30\,000$ cm^{-1} . The bolometer detects the depletion in beam flux when the laser is on resonance with an electronic transition. The noise in the bolometer signal (~ 100 nV $\text{Hz}^{-1/2}$) allows a beam depletion of ~ 1 part in 10^5 to be detected with unit signal-to-noise ratio. The optical radiation source was a frequency-doubled Ti:Al₂O₃ laser, which is a modified Indigo system³⁸ running with the Littman cavity³⁹ design. The Indigo is pumped by an Evolution-30,³⁸ a diode-pumped, intra-cavity frequency-doubled Nd:YLF laser. The second harmonic of the Ti:Al₂O₃ laser is generated by an angle-tuned lithium triborate (LBO) crystal. The laser can scan about 2000 cm^{-1} in the second harmonic region with a linewidth less than 0.2 cm^{-1} . The average pulse energy was about 150 μJ and the pulse width is ~ 10 ns. The laser fundamental wavelength was monitored by a Burleigh WA-4500 wavemeter.⁴⁰ The frequency calibration was achieved with a 7 cm^{-1} free spectral range etalon and a Ni–Ne hollow cathode optogalvanic lamp. Due to the limited frequency response of the bolometer, the 1 kHz repetition rate of the laser was reduced to 250 Hz by modulation with a chopper. The control of the laser system and data acquisition were performed with a PC running a custom program written in Labview.⁴¹

Normal modes were calculated by the density functional theory (DFT) using the BP86 functional in the ground electronic state and time-dependent density functional theory (TD-DFT) in the first excited state using the def-SV(P) basis set. The Turbomole package was used for these calculations.^{42,43} The energy and oscillator strength of the low-lying electronic transitions were calculated at the TD-DFT level using the B3LYP functional. The Gaussian 03 package was used for these calculations.⁴⁴ The MolFC program was used to calculate the Franck–Condon factors.⁴⁵

3. Results

3.1 Electronic spectroscopy of benzo[*g,h,i*]perylene inside helium nanodroplets

The electronic spectrum of BghiP inside helium nanodroplets is presented in the top section of Fig. 1. The peak at 25 024.7 cm^{-1} is assigned as the origin of the $S_1 \leftarrow S_0$ transition and the broad peak around 27 000 cm^{-1} is assigned to the origin of the

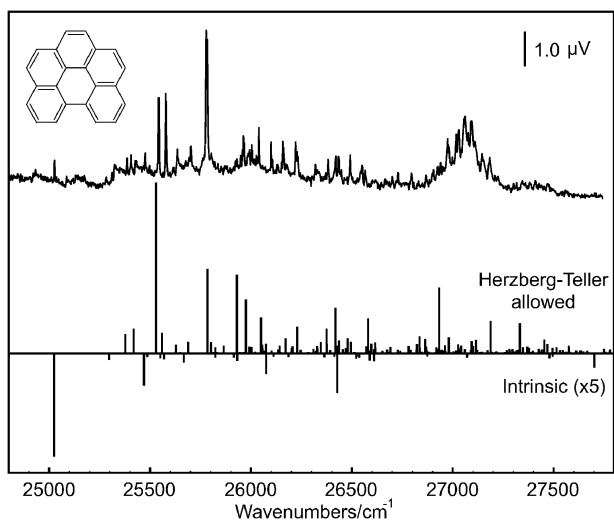


Fig. 1 Experimental (top) and simulated (bottom) electronic spectra of BghiP inside helium nanodroplets. The pickup oven temperature was 177 °C.

$S_2 \leftarrow S_0$ electronic transition in agreement with the gas-phase spectra.^{29,31} The broad structure which the $S_1 \leftarrow S_0$ transition rides on is due to the droplets loaded with BghiP dimers. The dimer assignment is based on the spectroscopy of PTCDA oligomers in helium nanodroplets carried out by the Stienkemeier group¹² and our explicit study of the pressure dependence of the perylene depletion signal.⁴⁶ The fact that the $S_1 \leftarrow S_0$ and $S_2 \leftarrow S_0$ electronic transitions are observed with comparable intensity despite the large difference in their theoretical transition dipole moments indicates strong vibronic coupling *via* the b_1 modes.

We have calculated the first order Herzberg–Teller (HT) coupling activities of the b_1 modes following the procedure reported before.¹⁹ These active modes are combined with the Franck–Condon factors of the a_1 modes calculated using the MolFC program.⁴⁵ S_1 normal modes, calculated by TD-DFT with the def-SV(P) basis set, were kindly provided by Tan.²⁹ The simulated $S_1 \leftarrow S_0$ stick spectrum is presented also in Fig. 1. The negative sticks are the direct intrinsic transitions, which include the electronic origin and several totally symmetric modes. The intensities of these transitions are scaled to match the experimental intensity of the origin and are shown with 5 times amplification. The positive sticks are the Herzberg–Teller allowed transitions which originate from the b_1 modes and include totally symmetric modes built on these b_1 “false origins”. The simulation successfully identifies the normal modes involved in intensity borrowing although the relative intensities are not perfectly reproduced, most notably, for the two strong peaks around 25 500 cm^{-1} : the $3b_1$ and the $4b_1$ modes. The complete list of peak positions and assignments are given in Table 1. A comparison to gas-phase positions reveals a mean helium matrix shift of only 2–3 cm^{-1} which indicates a very similar solvation energy for the ground and the excited states. The signal-to-noise ratio of the HENDI spectrum is improved over the published gas-phase one. In that work, only HT-induced transitions to S_1 were assigned; in the HENDI spectrum we can also assign some

weak transitions that are assigned to excitation of only the totally symmetric modes, which implies they arise from the weak intrinsic S_1 transition strength.

The detailed view of the typical S_1 peaks is presented in Fig. 2. The characteristic peaks of BghiP have split ZPLs separated by $\sim 1.9 \text{ cm}^{-1}$ with the blue one about 30–50% higher intensity. The FWHM of the peaks are ~ 1.0 and $\sim 1.5 \text{ cm}^{-1}$ for the red and the blue ZPLs respectively. The phonon wing is very weak. The peak shape does not depend significantly on the vibrational excess energy (up to $\sim 1000 \text{ cm}^{-1}$), although the red component of the electronic origin is narrower (FWHM $\sim 0.5 \text{ cm}^{-1}$). We note that the splitting observed in these spectra are due to the helium environment and the splitting presented in the gas-phase spectra are due to the rotational contours.³¹ The rotational temperature of the molecule in the supersonic expansion is about 40 K³¹ whereas in helium nanodroplets it is 0.4 K. In our spectrum, the perylene (and also coronene) impurity lines are weak compared to the gas-phase spectrum and peaks are easily distinguishable due to the characteristic peak shapes of these molecules inside helium droplets, *i.e.* coronene has one peak, BghiP has two peaks and perylene has one peak with a strong and broad phonon wing. In the case of perylene (and perhaps also coronene), the high emission quantum yield reduces the sensitivity when observed in beam depletion.

A detailed comparison of the S_2 origin spectrum in the gas phase and in helium droplets is presented in Fig. 3. The width of the feature reflects the very rapid $S_2 \rightarrow S_1$ internal conversion; the individual peaks are mainly S_1 vibronic levels that are enhanced by their near mixing with the strong, nearly degenerate S_2 origin. The comparison of the HENDI and gas-phase spectra reveals that the individual peaks are in excellent registration, as expected by the very small shift of S_1 vibronic transitions. However, the center of gravity of the S_2 feature has redshifted by about 40 cm^{-1} ; this represents the greater solvation energy of the S_2 state relative to S_1 and S_0 . The FWHM of the S_2 origin is 168 cm^{-1} , which corresponds to a lifetime of 32 fs. This width compares well with the spectra taken in other cryogenic matrices, *i.e.* $\sim 200 \text{ cm}^{-1}$ in neon²⁷ and $\sim 375 \text{ cm}^{-1}$ in argon.³¹ Qualitatively, the molecule relaxes faster in the environment with stronger interaction. There is a moderate broadening of the transitions in the helium clusters compared to the gas phase. This is most likely due to the fact that the vibrational relaxation in helium droplets is faster than the electronic relaxation. It was demonstrated before that the emission of similar aromatic molecules is exclusively from the ground level of the S_1 state.¹⁰

3.2 Van der Waals complexes of benzo[*g,h,i*]perylene with argon and oxygen

We have made clusters of BghiP with argon and oxygen inside helium droplets with consecutive pickup events. Fig. 4 shows the spectrum of BghiP with argon for the transitions $3b_1$ and $4b_1$. We could only observe a single peak at -8.4 cm^{-1} from the blue ZPLs with increasing argon pressure. This peak is assigned as the 1:1 complex. An unexpected feature of the spectrum is that the higher energy (and initially more intense) monomer peak decreases faster with Ar pressure than does the

Table 1 Observed line positions and assignments for $S_1 \leftarrow S_0$ transition of *BghiP* inside helium nanodroplets. (All values in cm^{-1} , strong lines are indicated with bold typeface)

Position	FWHM	Splitting	Vibrational excess	Simulation ^a	Gas phase position ^b	Assignments ^c
25 024.7	0.5	1.9	0.0	25 024.7	25 027.1	Origin
25 026.6	1.3					
25 331.0			306.3	25 297.0		272.3 (1a ₁) ₀ ¹
25 384.7	1.0	1.8	360.0	25 377.6	25 386.0	252.9 (1b ₁) ₀ ¹
25 386.5	1.0					
25 404.0	0.9	1.9	379.3	25 419.2	24 405.3	394.5 (2b ₁) ₀ ¹
25 405.9	1.5					
25 473.5	0.7	1.5	448.8	25 469.9		445.2 (3a ₁) ₀ ¹
25 475.0	0.9		450.3			
25 496.1	1.3	2.0	471.4	25 486.5		461.8 (4a ₁) ₀ ¹
25 498.1	1.4		473.4			
25 542.0	1.0	1.9	517.3	25 529.6	25 544.6	504.9 (3b ₁) ₀ ¹
25 543.9	1.3		519.2			
25 577.3	1.0	2.0	552.6	25 558.4	25 579.8	533.7 (4b ₁) ₀ ¹
25 579.3	1.5		554.6			
25 635.9			611.2	25 628.2		603.4 (5b ₁) ₀ ¹
25 700.8	1.0	1.9	676.1	25 689.4		664.7 (6b ₁) ₀ ¹
25 702.7	1.6		678.0			
25 777.2	1.7	1.9	752.5	25 784.2	25 776.8	759.5 (7b ₁) ₀ ¹
25 779.1	1.0		754.4			
25 780.7	1.0		756.0			
25 782.8	2.3		758.1			
25 784.8	1.3		760.1		25 784.2	
25 785.4	4.6		760.7			
25 804.5			779.8	25 801.9		504.9 (3b ₁)

Table 1 (continued)

Position	FWHM	Splitting	Vibrational excess	Simulation ^a	Gas phase position ^b	Assignments ^c
26 490.5	1.0	1.6	1465.8	26 495.0		1025.2 (10b ₁) ₀ [†] + 445.2 (3a ₁) ₀ [†]
26 492.2	0.9		1467.5			
26 493.3	3.4		1468.6			
26 545.4	4.6	2.5	1520.7			
26 547.1	0.3		1522.4			
26 549.6	0.8		1524.9			
26 551.3	1.0	1.6	1526.6	26 580.9		504.9 (3b ₁) ₀ [†] + 525.7 (5a ₁) ₀ [†]
26 552.9	0.5		1528.2			
26 554.6	2.8		1529.9			
26 564.1	1.2	1.9	1539.4			
26 566.0	1.3		1541.3			
26 567.9	1.0		1543.2			
26 570.0	2.4	1.9	1545.3			
26 728.1	1.8		1703.4			
26 730.0	2.0		1705.3			

^a Calculated with normal mode wavenumbers (given in the assignment column) and HENDI origin position. ^b From ref. 31. ^c Calculated by Tan and Salama.²⁹

lower energy peak. It is generally assumed that the capture of solutes by the helium droplets occurs before complexation with an already present species and thus the rate of decrease of the monomer spectral features is expected to decrease at the same rate, regardless of the local helium solvation structure that is likely responsible for the multiple ZPLs. We can offer two possible explanations. It is possible that the relative formation probability of the two different helium solvation structures could be helium droplet-size dependent, as this affects the rate of droplet cooling after pickup. If the higher energy peak is stronger in larger droplets, then it could be expected to decrease faster with Ar pressure since those droplets will have a higher Ar pickup cross section. An alternative explanation is that some of the Ar collisions do not lead to Ar pickup but do heat the droplets and this could lead to an annealing of the helium solvation structure around the already solvated *BghiP*.

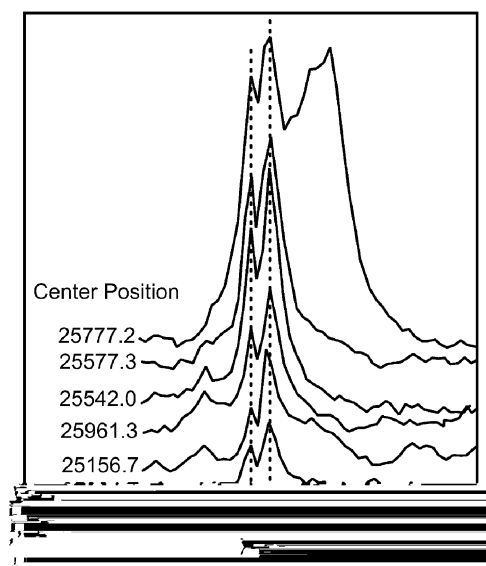


Fig. 2 Lineshapes of the *BghiP* S₁ ← S₀ transition for various vibronic bands. Peak centers are indicated next to curves.

Fig. 5 shows the same spectral region with increasing O₂ pressure. The weak doublet structure, located −17.2 cm^{−1} from the blue ZPLs, is assigned as the 1 : 1 oxygen complex. The complex peak shows increased linewidths and an increase in the splitting from 1.7 to 2.0–3.4 cm^{−1}. Both components of the complex seem to have equal intensity. A second peak (FWHM: 1.3 cm^{−1}), positioned 33.8 cm^{−1} to the red of the blue ZPL, shows up with increasing O₂ pressure. For the main peak at 25 880 cm^{−1} this new complex peak is hidden under the blue ZPL of the peak around 25 540 cm^{−1}, indicated by the different ZPL intensity ratios of these two *BghiP* peaks. The new peak, which does not show any splitting, is assigned as the 1 : 2 complex.

In the pickup of O₂, the two ZPL lines decrease with similar rates, unlike the Ar pickup considered above. This suggests that droplet size is not the determinant factor.

Although we could observe a complex of 2 oxygen molecules with 1 *BghiP* molecule, the corresponding complex was not detected for the argon case. While the exact reasons are

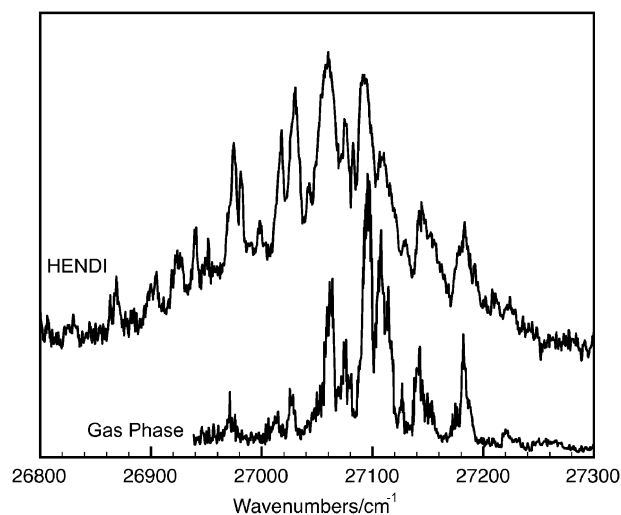


Fig. 3 Detailed view of the S₂ ← S₀ transition origin of *BghiP* inside helium droplets and in the gas phase.

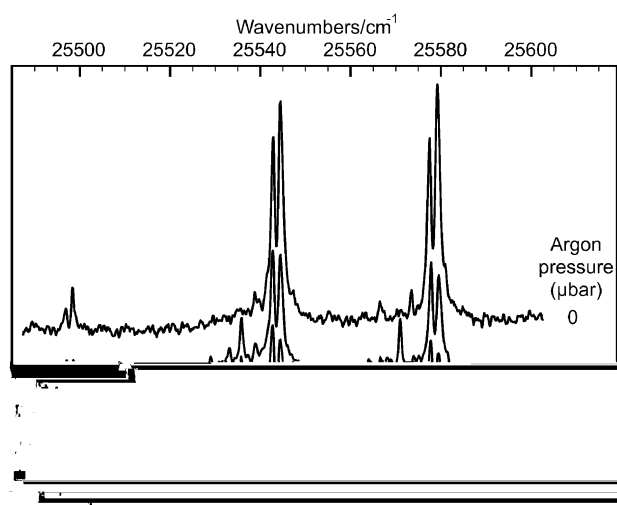


Fig. 4 BghiP–argon complex inside helium droplets at 3b₁ and 4b₁ manifolds. Argon pressure is measured outside the chamber.

not clear, we can point out that a broad background emerges with increasing argon pressure. It was demonstrated before that the depletion signal of oxygen containing complexes may be enhanced.¹⁷ The contrast observed here could be attributed to the fluorescence quenching behaviour of oxygen.

3.3 Electronic spectroscopy of coronene inside helium nanodroplets

The electronic spectrum of coronene inside helium droplets is presented in Fig. 6. The transition is a forbidden transition induced by e_{2g} modes. The spectrum consists of sharp ZPLs (FWHM: ~0.4 cm⁻¹) and accompanying very weak PWs. In general, the spectrum is similar to previously observed gas-phase LIF spectrum. The strongest peak, which was previously observed as a single line, is now resolved into several transitions. In addition, the weaker lines in HENDI spectrum are enhanced compared to the gas phase.

A list of the observed transitions and comparison to gas-phase measurements is presented in Table 2. In contrast to the gas-phase measurements, we did not detect weak lines between the peaks indexed as a and i. The weak (impurity) peak around 24 555 cm⁻¹ has a FWHM of ~7 cm⁻¹, which is quite larger than the typical coronene peaks.

We have simulated the S₁ ← S₀ transition of coronene using the calculated e_{2g} and a_{1g} normal modes, MolFC program and TD-DFT.¹⁹ The simulated spectrum is given in the bottom part of Fig. 6. The simulation can account for most of the strong transitions. However, the group of low intensity peaks around the strong peaks cannot be explained by the first order approximation presented here. In addition, the simulation predicts significant intensity for the e_{2g} mode at 25 286 cm⁻¹ while the experiment does not reproduce this.

3.4 Van der Waals complexes of coronene with argon and oxygen

Fig. 7 shows the S₁ ← S₀ transition of the coronene–argon complex inside helium nanodroplets near the parent peak labeled as “p”. We initially observed two peaks, which are

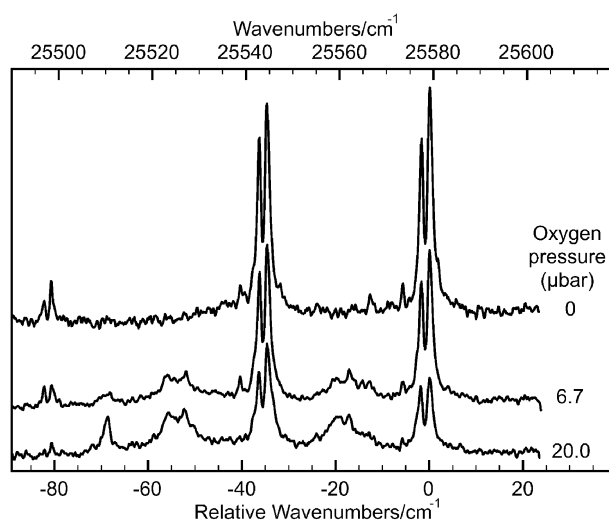


Fig. 5 BghiP–oxygen complex inside helium droplets at 3b₁ and 4b₁ manifolds. Oxygen pressure is measured outside the chamber.

assigned as the 1 : 1 complex peaks, at -2.98 and -4.12 cm⁻¹. Due to the high symmetry of coronene, there are two distinct positions where argon can localize. Statistically one would expect a 1 : 6 intensity ratio for these two complexes. The intensity ratio approaches this limit only at sufficiently high argon pickup pressures. The peak, redshifted by 4.12 cm⁻¹, is assigned to the complex where the argon is localized on one of the outer rings. Consequently, the peak redshifted by 2.98 cm⁻¹ is assigned to the complex where the argon is localized over the central ring. A third peak shows up with increasing argon pressure at 9.73 cm⁻¹ to the red of the parent peak. This peak is assigned as the 1 : 2 complex. It is, however, not easily distinguishable where the two argon atoms are located over the coronene ring.

Fig. 8 shows the same spectral region with oxygen in the pickup cell. In this case, we observed two complex peaks 3.32 and 7.94 cm⁻¹ redshifted from the parent peak. The more

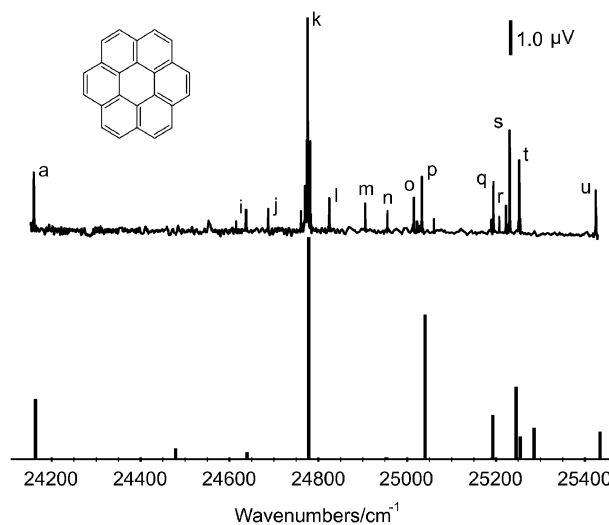


Fig. 6 Experimental (top) and simulated (bottom) electronic spectra of coronene inside helium nanodroplets. The pickup oven temperature was 175 °C.

Table 2 Positions and linewidths for the peaks of the $S_1 \leftarrow S_0$ transition of coronene in helium nanodroplets (all values in cm^{-1})

Index ^a	Gas phase ^b	HENDI	FWHM	Shift	Excess	Calculation ^c
a	24 061.4					
b	24 176.1					
c	24 300.8					
d	24 349.3					
e	24 373.1					
f	24 407.1					
g	24 447.1					
h	24 492.6					
i	24 566.7					
j	24 596.4					
	24 625.5					
	24 646.2					
i	24 652.2	24 636.6	0.40	-15.6	828.6	355.7 ($12e_{2g}$) ₀ ¹
		24 637.6	0.40		829.6	
j	24 698.6	24 687.1	0.43	-11.53	879.1	
		24 761.2	0.36		953.2	
		24 769.6	0.53		961.6	
		24 774.6	1.22		966.6	
k	24 791.7	24 775.8	0.36	-15.9	967.8	970.8 ($9e_{2g}$) ₀ ¹
		24 782.3	0.40		974.3	
l	24 836.1	24 824.5	0.50	-11.6	1016.5	
m	24 917.9	24 905.5	0.40	-12.4	1097.5	
n	24 966.5	24 955.4	0.37	-11.1	1147.4	1132.4 ($8e_{2g}$) ₀ ¹
	25 009.6					
o	25 034.0	25 015.2	0.40	-18.8	1207.2	1232.4 ($7e_{2g}$) ₀ ¹
p	25 046.6	25 032.8	0.32	-13.8	1224.8	
	25 073.0	25 060.1	0.43	-12.9	1252.1	
	25 133.6					
		25 189.1	0.38		1381.1	
		25 189.9	0.49		1381.9	
q	25 209.7	25 193.8	0.43	-15.9	1385.8	1384.9 ($6e_{2g}$) ₀ ¹
	25 221.8	25 207.4	0.37	-14.4	1399.4	
r	25 236.4	25 222.3	0.42	-14.1	1414.3	
s	25 246.0	25 230.4	0.58	-15.6	1422.4	1437.3 ($5e_{2g}$) ₀ ¹
t	25 267.1	25 252.1	0.51	-15.0	1444.1	970.8 ($9e_{2g}$) ₀ ¹ + 475.7 ($6a_{1g}$) ₀ ¹
u	25 442.1	25 424.1	0.39	-18.0	1616.1	1626.6 ($3e_{2g}$) ₀ ¹
		25 425.2	0.52		1617.2	

^a As used in ref. 33. ^b From ref. 33; calculated as the sum of the reported origin ($23\,808\text{ cm}^{-1}$) and the reported gas-phase vibrational excess. One gets slightly different values if the reported (air) wavelengths are converted to wavenumbers. ^c TD-DFT with def-SV(P) basis set.

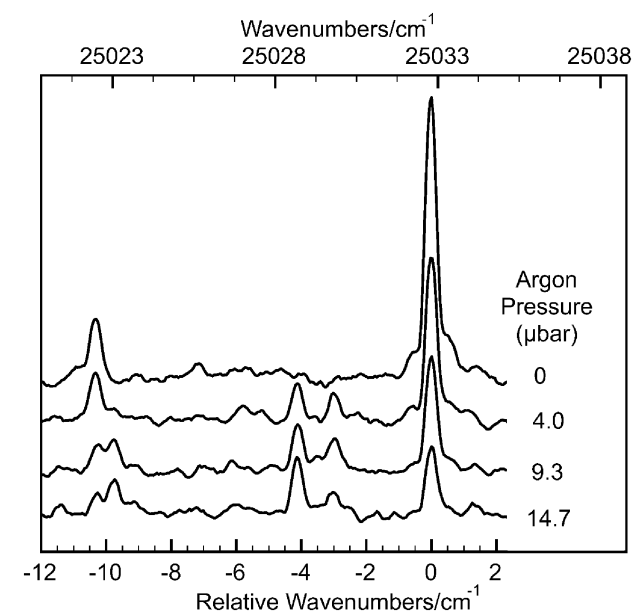


Fig. 7 Coronene-argon complex inside helium droplets at peak "p".

redshifted peak is always more intense than the other one, thus it is assigned to the complex where oxygen is localized over the outer rings. This peak is also asymmetric on the blue side, which probably arises because of different orientations of the oxygen molecule on coronene. Despite our efforts we could not observe complexes with more than one oxygen molecule.

4. Discussions

Although the first order Herzberg-Teller approximation can satisfactorily account for the spectrum of $BghiP$, it is not as successful in the case of coronene. The presence of groups of weak peaks around the strong inducing modes suggests that there is some mechanism for redistributing the intensity, perhaps anharmonic coupling in S_1 or S_1-T_1 coupling. In addition, some of these weak peaks could be due to the presence of ^{13}C isotopes in coronene, which will lower the symmetry and cause shifts in the normal modes. We have done electron structure calculations for substituted ^{13}C on coronene molecule without removing the symmetry, *i.e.* 6 C atoms at a time for the inner and the medium rings and 12 C atoms at a time for the outer ring, and calculated the normal modes in the

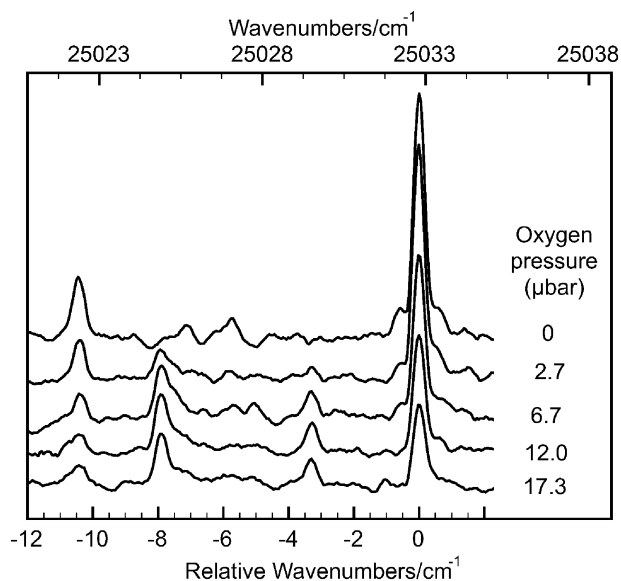


Fig. 8 Coronene–oxygen complex inside helium droplets at peak “p”.

S_0 and S_1 states.⁴⁷ We have confirmed that most of the satellite peaks do not have the expected shift. The satellite peaks which are within the expected shifts have intensities more than the expected based on the abundance of ^{13}C as shown for the “k” peak satellites in Fig. 9. Thus we conclude that isotopic contamination is not responsible for the unassigned lines in the spectrum.

A summary of observed peak shapes for the aromatic molecules studied inside helium droplets is given in Table 3.

Initially, it was proposed that the localization of helium atoms over the molecular surface would give rise to different structural isomers of the first solvation shell and cause splitting of the ZPLs.⁶ Later, detailed experiments and calculations performed on helium-solvated tetracene⁶ and phthalocyanine^{13–15,48} suggested that actually both the ground and the excited states of these molecules are split into two levels. The exact mechanism of splitting and whether it is molecule-

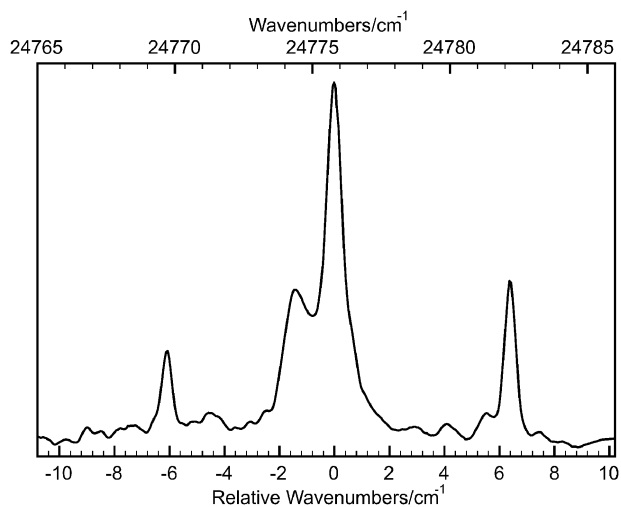


Fig. 9 Detailed view of coronene “k” peak.

Table 3 Summary of spectral properties for electronic excitation of aromatic molecules inside helium nanodroplets

Molecule	No. of ZPLs	PW
Benzene ^{1,2}	1	–
Naphthalene ³	1	–
Anthracene ⁴	>2	+ ^d
Tetracene ^{5–10}	2	+ ^e
Pentacene ^{5,9,10}	1	+ ^f
Perylene ^{10,17,23}	>2	+ ^g
Benzo[<i>g,h,i</i>]perylene ^j	2	–
Coronene ^j	1	–
Phthalocyanine ^{9,14–16}	1 ^a 3 ^b	+
Mg–phthalocyanine ¹⁵	3 ^a 2 ^b	+
Biphenylene ¹⁹	2	+ ^e
Acenaphthylene ²⁰	>2	+ ^h
Fluoranthene ²⁰	1	+
Benzo(k)fluoranthene ²⁰	2 ^c	+ ⁱ

^a Excitation. ^b Emission. ^c Until 1500 cm^{-1} vibrational excess. ^d No gap after ZPLs. ^e With characteristic gap. ^f With fine structure. ^g Weak when detected by LIF, strong when detected by beam depletion. ^h Broad. ⁱ Broad for 0–0 transition, weak for vibronic transitions. ^j This work.

specific or not is still unclear. In the solvation model there are a small number of isomers, since the localization is more effective for the first solvation layer. Path integral Monte Carlo calculations of benzene in a He_{39} cluster predicted that the He atoms above and below the plane of the molecule are completely localized.⁴⁹ Quantum Monte Carlo calculations of interaction of helium (up to 24 atoms) with planar polycyclic aromatic molecules also found a strong localization of helium in the first solvent layer above and below the rings.⁵⁰ Similarly, path integral Monte Carlo calculations of phthalocyanine in He_N ($N_{\text{max}} = 150$) clusters indicate a strong localization of the first solvation layer.⁴⁸ Because this first layer of helium is separated from the rest, this layer is considered to be non-superfluid. The appearance of the splitting pattern was reported to depend sensitively on the first solvation layer. Addition of an Ar atom to the tetracene molecule quenched the splitting completely.⁵ We have demonstrated in our laboratory that biphenylene, which also has split ZPLs, retained the splitting upon complexation with an argon atom unlike the tetracene case.¹⁹ It should be noted that the separation of minima positions (*i.e.* the center of benzene rings) is 3.85 Å for biphenylene as compared to 2.5 Å for tetracene, whereas the equilibrium distance of the helium dimer is 2.96 Å.⁵¹

In previous works involving large aromatic molecules,^{19,20} we employed potential energy surfaces generated by summation of pairwise interactions based on benzene molecule due to the lack of *ab initio* potentials. Also demonstrated by the Monte Carlo simulations mentioned above, the interaction of a single helium atom with a large polycyclic molecule is regarded as descriptive of the environment of a molecule inside helium droplets.⁴⁸ We have used the angle-dependent Lennard-Jones potential (6–12 for H–X; 8–14- θ for C–X), which was used by the Whaley group⁴⁹ to fit the MP2 level benzene–helium potential calculation of Hobza *et al.*⁵² We scaled the parameters ($\epsilon_{\text{C–Ar}} = 60.59 \text{ cm}^{-1}$, $\epsilon_{\text{H–Ar}} = 76.05 \text{ cm}^{-1}$, $\sigma_{\text{C–Ar}} = 3.81 \text{ Å}$ and $\sigma_{\text{H–Ar}} = 2.86 \text{ Å}$) to reproduce the most

recent CCSD(T) level benzene–argon calculation:⁵³

$$E_{C-X}(\vec{r}) = 4\epsilon_{C-X} \cos^2 \theta \left[\left(\frac{\sigma_{C-X} \cos \theta}{|\vec{r}|} \right)^{14} - \left(\frac{\sigma_{C-X} \cos \theta}{|\vec{r}|} \right)^8 \right]$$

$$E_{H-X}(\vec{r}) = 4\epsilon_{H-X} \left[\left(\frac{\sigma_{H-X}}{|\vec{r}|} \right)^{12} - \left(\frac{\sigma_{H-X}}{|\vec{r}|} \right)^6 \right]$$

$$E_{\text{molecule-X}}(\vec{r}) = \sum E_{C-X}(\vec{r} - \vec{r}') + \sum E_{H-X}(\vec{r} - \vec{r}')$$

where θ is defined as the angle between the H–X or C–X vector and the vector perpendicular to the molecular surface. A comparison of the results of this fit and the CCSD(T) calculations was reported previously.¹⁹

The coronene–argon van der Waals complex shows two peaks for the low pickup pressure regime. Based on the intensity ratio, the peaks redshifted by 2.98 and 4.12 cm^{-1} have been assigned to the argon localized above the center ring and above one of the outer rings respectively. A pairwise computation of the coronene–argon interaction places the absolute minima over the center of an outer ring with a well depth of 355.8 cm^{-1} at 3.60 Å. The local minimum is located 3.63 Å above the center ring at a depth of 336.4 cm^{-1} . Fig. 10 is the 2-D contour plot of the interaction calculated at the equilibrium distance. Although the calculation is in agreement with the observations and assignments, it should be kept in mind that in this model the well depth of the He and Ar with H is larger than for the same with C, which is responsible for the deeper well for the center of outer rings compared to the central ring.

The 1:2 complex peak appears at -9.73 cm^{-1} , which is slightly larger than twice the 1:1 complex shift. We could not find a similar study in the gas phase for the S_1 manifold. However, the Topp group studied the coronene–argon van der Waals complexes at the S_2 manifold.⁵⁴ They observed only one

peak for the 1:1 complex redshifted by 24 cm^{-1} with a width of 7 cm^{-1} . It is possible that the information about the two distinct argon positions over the ring could be washed out due to the lifetime broadening of the peak. The 1:2 complex is redshifted by 48.5 cm^{-1} with the same width. Furthermore, they reported that the shifts increase linearly as a function of the number

of shell is

previously observed with perylene–argon clusters at the S_1 manifold.⁵⁵ The shift continues to be linear after the first solvation shell, but with a different dependence factor. We point out that it is possible for the shifts for the helium solvated coronene–argon system at the S_1 manifold to be (almost) linear, as we observed previously for the benzo(k)-fluoranthene–argon system inside the helium nanodroplets.²⁰

The distinction between the center and the outer rings of coronene

ff742heff

of

Acknowledgements

This work was funded by National Science Foundation and by the University of Virginia. We thank Giacinto Scoles for his support and suggestions. We thank Xiaofeng Tan for providing the gas-phase electronic spectrum and the normal mode displacements in both S_0 and S_1 of BghiP which allowed us to predict the vibronic structure in the spectrum. We thank Alkwin Slenczka for helpful comments on the manuscript.

References

- 1 R. Schmied, P. Çarçabal, A. M. Dokter, V. P. A. Lonij, K. K. Lehmann and G. Scoles, *J. Chem. Phys.*, 2004, 121, 2701–2710.
- 2 A. Boatwright, N. A. Besley, S. Curtis, R. R. Wright and A. J. Stace, *J. Chem. Phys.*, 2005, 123, 021102.
- 3 A. Lindinger, PhD Thesis, *Vibronische Spektroskopie von organischen und biologischen Molekülen in $^4\text{Helium-Clustern}$* , Georg-August-Universität, 1999.
- 4 S. Krasnokutski, G. Rouillé and F. Huisken, *Chem. Phys. Lett.*, 2005, 406, 386–392.
- 5 M. Hartmann, A. Lindinger, J. P. Toennies and A. F. Vilesov, *Chem. Phys.*, 1998, 239, 139–149.
- 6 M. Hartmann, A. Lindinger, J. P. Toennies and A. F. Vilesov, *J. Phys. Chem. A*, 2001, 105, 6369–6377.
- 7 A. Lindinger, J. P. Toennies and A. F. Vilesov, *Phys. Chem. Chem. Phys.*, 2001, 3, 2581–2587.
- 8 P. Pörtner, A. F. Vilesov and M. Havenith, *Chem. Phys. Lett.*, 2001, 343, 281–288.
- 9 M. Hartmann, A. Lindinger, J. P. Toennies and A. F. Vilesov, *Phys. Chem. Chem. Phys.*, 2002, 4, 4839–4844.
- 10 R. Lehnig and A. Slenczka, *J. Chem. Phys.*, 2005, 122, 244317.
- 11 M. Wewer and F. Stienkemeier, *J. Chem. Phys.*, 2003, 120, 1239–1244.
- 12 M. Wewer and F. Stienkemeier, *Phys. Rev. B*, 2003, 67, 125201.
- 13 R. Lehnig and A. Slenczka, *J. Chem. Phys.*, 2003, 118, 8256–8260.
- 14 R. Lehnig and A. Slenczka, *J. Chem. Phys.*, 2004, 120, 5064–5066.
- 15 R. Lehnig and A. Slenczka, *ChemPhysChem*, 2004, 5, 1014–1019.
- 16 R. Lehnig, A. Joshua, J. A. Sebree and A. Slenczka, *J. Phys. Chem. A*, 2007, 111, 7576–7584.
- 17 P. Çarçabal, R. Schmied, K. K. Lehmann and G. Scoles, *J. Chem. Phys.*, 2004, 120, 6792–6793.
- 18 A. Staicu, S. Krasnokutski, G. Rouillé, T. Henning and F. Huisken, *J. Mol. Struct.*, 2006, 786, 105–111.
- 19 Ö. Birer, P. Moreschini, K. K. Lehmann and G. Scoles, *J. Phys. Chem. A*, 2007, 111, 7624–7630.
- 20 Ö. Birer, P. Moreschini, K. K. Lehmann and G. Scoles, *J. Phys. Chem. A*, 2007, 111, 12200–12209.
- 21 G. Rouillé, S. Krasnokutski, F. Huisken, T. Henning, O. Sukhorukov and A. Staicu, *J. Chem. Phys.*, 2004, 120, 6028–6034.
- 22 M. Hartmann, F. Mielke, J. P. Toennies, A. F. Vilesov and G. Benedek, *Phys. Rev. Lett.*, 1996, 76, 4560–4563.
- 23 J. P. Higgins, PhD Thesis, *Helium Cluster Isolation Spectroscopy*, Princeton University, 1998.
- 24 E. J. Bowen and B. Brocklehurst, *J. Chem. Soc.*, 1954, 3875–3878.
- 25 T. B. Tamm and P. M. Saari, *Chem. Phys. Lett.*, 1975, 30, 219–222.
- 26 L. A. Nakhimovsky, M. Lamotte and J. Jousot-Dubien, *Handbook of low temperature electronic spectra of polycyclic aromatic hydrocarbons*, Elsevier, New York, NY, 1989.
- 27 X. Chillier, P. Boulet, H. Chermette, F. Salama and J. Weber, *J. Chem. Phys.*, 2001, 115, 1769–1776.
- 28 N. Nijegorodov, R. Mabbs and W. S. Downey, *Spectrochim. Acta, Part A*, 2001, 57, 2673–2685.
- 29 X. Tan and F. Salama, *J. Chem. Phys.*, 2005, 123, 014312.
- 30 P. Moreschini, Ö. Birer and K. K. Lehmann, Electronic Spectroscopy of Coronene and Benzoperylene in Helium Nanodroplets, at the *International Symposium on Molecular Spectroscopy 61st Meeting*, Ohio State University, Columbus, Ohio, June, 2006, pp. 19–23. Abstract and slides can be downloaded from http://molspect-chemistry.ohio-state.edu/symposium_61/symposium/Program/MI.html#MI02.
- 31 G. Rouillé, M. Arold, A. Staicu, S. Krasnokutski, F. Huisken, T. Henning, X. Tan and F. Salama, *J. Chem. Phys.*, 2007, 126, 174311.
- 32 D. M. Grebenshchikov and N. A. Kovrizhnykh, *J. Appl. Spectrosc.*, 1972, 16, 728–731.
- 33 G. Bermudez and I. Y. Chan, *J. Phys. Chem.*, 1986, 90, 5029–5034.
- 34 G. Bermudez and I. Y. Chan, *J. Phys. Chem.*, 1987, 91, 4710–4714.
- 35 C. Callegari, K. K. Lehmann, R. Schmied and G. Scoles, *J. Chem. Phys.*, 2001, 115, 10090–10110.
- 36 E. L. Knuth, B. Schilling and J. P. Toennies, in *19th International Symposium on Rarefied Gas Dynamics*, ed. J. Harvey and G. Lord, Oxford University Press Inc., Oxford, 1994, vol. 19, pp. 270–2751.
- 37 Infrared Laboratories, Tucson, AZ.
- 38 Positive Light Inc., Los Gatos, CA.
- 39 M. G. Littman, *Opt. Lett.*, 1978, 3, 138–140.
- 40 EXFO Burleigh Products Group Inc., Victor, NY.
- 41 National Instruments Corp., Austin, TX.
- 42 R. Ahlrichs, M. Bär, M. Häser, H. Horn and C. Kölmel, *Chem. Phys. Lett.*, 1989, 162, 165–169.
- 43 S. Boecker, P. Deglmann, F. Furche and M. Häser, *Turbomole*, Universität Karlsruhe, Germany.
- 44 M. J. Frisch, G. W. Trucks, H. B. Schlegel, G. E. Scuseria, M. A. Robb, J. R. Cheeseman, J. A. Montgomery, Jr., T. Vreven, K. N. Kudin, J. C. Burant, J. M. Millam, S. S. Iyengar, J. Tomasi, V. Barone, B. Mennucci, M. Cossi, G. Scalmani, N. Rega, G. A. Petersson, H. Nakatsuji, M. Hada, M. Ehara, K. Toyota, R. Fukuda, J. Hasegawa, M. Ishida, T. Nakajima, Y. Honda, O. Kitao, H. Nakai, M. Klene, X. Li, J. E. Knox, H. P. Hratchian, J. B. Cross, V. Bakken, C. Adamo, J. Jaramillo, R. Gomperts, R. E. Stratmann, O. Yazyev, A. J. Austin, R. Cammi, C. Pomelli, J. Ochterski, P. Y. Ayala, K. Morokuma, G. A. Voth, P. Salvador, J. J. Dannenberg, V. G. Zakrzewski, S. Dapprich, A. D. Daniels, M. C. Strain, O. Farkas, D. K. Malick, A. D. Rabuck, K. Raghavachari, J. B. Foresman, J. V. Ortiz, Q. Cui, A. G. Baboul, S. Clifford, J. Cioslowski, B. B. Stefanov, G. Liu, A. Liashenko, P. Piskorz, I. Komaromi, R. L. Martin, D. J. Fox, T. Keith, M. A. Al-Laham, C. Y. Peng, A. Nanayakkara, M. Challacombe, P. M. W. Gill, B. G. Johnson, W. Chen, M. W. Wong, C. Gonzalez and J. A. Pople, *GAUSSIAN 03 (Revision C.02)*, Gaussian, Inc., Wallingford, CT, 2004.
- 45 R. Borrelli and A. Peluso, *MolFC: A program for Franck–Condon integrals calculation*, 2004.
- 46 Ö. Birer, P. Moreschini and K. K. Lehmann, unpublished data.
- 47 There are two sources for the observed shift. The first one is the difference in the zero point energies (ZPE). The expected shift, which should be observed on all modes, is the calculated shift divided by the number of substituted carbon atoms, assuming the shifts will be additive as in the first-order perturbation theory. This shift is 1.2, 6.9, 1.4 cm^{-1} for the inner (I), middle (II) and outer (III) identical C ring substitutions respectively. The second one is the isotopic shift in the normal modes. In this case, the expected shift is again the calculated shift divided by the number of carbon atoms. However, for the doubly degenerate e_{2g} modes, one of the modes is going remain at the original frequency (therefore it will shift only due to the changes in the ΔZPEs) and the second one is going to shift twice the expected value. The expected shifts for $12e_{2g}$, $9e_{2g}$, $7e_{2g}$, $6e_{2g}$, $5e_{2g}$ and $3e_{2g}$ modes are (I) 0.5, -6.0 , 0.7, -1.5 , 0.5, -5.6 ; (II) 5.5, 7.1, 0.2, -2.7 , 3.9, 2.5; and (III) 0.0, -0.5 , -0.1 , 0.3, -3.8 , -1.9 cm^{-1} respectively.
- 48 H. D. Whitley, P. Huang, Y. Kwon and K. B. Whaley, *J. Chem. Phys.*, 2005, 123, 054307.
- 49 Y. Kwon and K. B. Whaley, *J. Chem. Phys.*, 2001, 114, 3163–3169.
- 50 P. Huang, H. D. Whitley and K. B. Whaley, *J. Low Temp. Phys.*, 2004, 134, 263–268.
- 51 A. R. Janzen and R. Aziz, *J. Chem. Phys.*, 1997, 107, 914–919.
- 52 P. Hobza, O. Bludsky, H. L. Selzle and E. W. Schlag, *J. Chem. Phys.*, 1992, 97, 335–340.
- 53 H. Koch, B. Fernandez and J. Makarewicz, *J. Chem. Phys.*, 1999, 111, 198–204.
- 54 R. J. Babbitt, C. J. Ho and M. R. Topp, *J. Phys. Chem.*, 1988, 92, 2422–2429.
- 55 D. Bahatt, A. Heidenreich, N. Benhorin, U. Even and J. Jortner, *J. Chem. Phys.*, 1994, 100, 6290–6299.